PNAS RESEARCH ARTICLE | CELL BIOLOGY
BIOPHYSICS AND COMPUTATIONAL BIOLOGY

Immune cells employ intermittent integrin-mediated traction forces for 3D migration

Tina Czerwinski[a], Lars Bischof[a], David Böhringer[a], Sibel Kara[b], Pamela L. Strissel[c,d,e,f], Reiner Strick[d,f], Natalie Huhn[a,g], Alexander Winterl[a], Richard Gerum[a], Ernst Wittmann[a], Michael Schneider[d,f], Matthias W. Beckmann[d,f], Gina Nusser[b], Manuel Wiesinger[f,h,i], Silvia Budday[j], Anja Lux[b], Caroline Voskens[f,h,i], Ben Fabry[a], and Christoph Mark[a,1]

Affiliations are included on p. 11.

Edited by Jason G. Cyster, Howard Hughes Medical Institute—University of California, San Francisco, CA; received September 2, 2025; accepted February 10, 2026

To reach targets outside the bloodstream, immune cells can extravasate and migrate through connective tissue. During tissue infiltration, immune cells migrate in an amoeboid fashion, characterized by weak matrix adhesions and low traction forces, that allows them to achieve high migration speeds of up to 10 μm/min. How immune cells reconcile amoeboid migration with the need to overcome steric hindrance in dense matrices is currently not understood. Here we show that NK92 (natural killer) cells can switch from their default amoeboid migration mode to a contractile, mesenchymal-like migration mode when moving through fibrous human amniotic membrane (HAM) tissue. We subsequently study immune cell migration in reconstituted 3D collagen networks with known mechanical properties and pore sizes and apply time-lapse confocal reflection microscopy to obtain simultaneous measurements of migration speed, directional persistence, and cell contractility. We find that NK92 cells exert substantial acto-myosin driven, integrin-mediated contractile forces of up to 100 nN on the extracellular matrix during short contractile phases. This burst-like contractile behavior is also found in primary B, T, NK cells, neutrophils, and monocytes, and is tightly related to the fraction of cells that become stuck in narrow pores of the surrounding matrix. Our results demonstrate that steric hindrance guides the rapid regulation of integrin-mediated adhesion to the ECM in a large number of immune cell subtypes.

cell migration | immune cells | traction forces | mechanosensitivity | collagen matrices

Significance

This study challenges the long-held notion that immune cells migrate through tissues without gripping the surrounding matrix, relying on a friction-based amoeboid migration mode. We show that when they face tight spaces within 3D matrices, human NK cells—as well as neutrophils, monocytes, B, and T cells—briefly switch gears: they engage integrin adhesions and generate short bursts of contractile force to deform the local microenvironment. Importantly, these intermittent, acto-myosin driven traction bursts are tightly related to the fraction of cells that become stuck in narrow matrix pores. Our findings revise the prevailing view of 3D leukocyte locomotion and suggest that tuning adhesion and cytoskeletal pathways could enhance immune infiltration of dense tissues and inform combinatorial cancer therapies.

Immune cells such as monocytes, neutrophilic granulocytes, as well as B cells, T cells, and natural killer (NK) cells can migrate through tissues up to 100 times faster than mesenchymal cells (1, 2). Immune cells typically use an amoeboid migration mode with limited or no proteolytic activity and limited or no specific (e.g. integrin-mediated) adhesion to the extracellular matrix (ECM) (3–5). Therefore, these cells are not expected to generate substantial traction forces, implying that they do not form mature focal adhesion contacts and thus are not able to significantly pull on and rearrange ECM fibers (4, 6). However, since migration in three-dimensional (3D) environments requires the cell to overcome the resistive forces of the matrix (7–9), some mechanism of force transmission across the plasma membrane to the ECM must exist but has not yet been characterized in these cells.

The involvement of integrins in leukocyte migration in 3D matrices has been studied previously, and the general conclusion is that integrins are required during extravasation but are not essential during tissue infiltration. For example, when integrin function is blocked in T cells, or when integrins are depleted in mouse dendritic cells, neutrophils, and B cells, migration is only possible in confined 3D environments but not on two-dimensional (2D) surfaces (2, 4). More specifically, integrin depletion in mouse leukocytes does not affect migration speed in 3D collagen gels, indicating that these cells do not require integrins for interstitial migration, whereas they do for migration on 2D substrates (2). Dendritic cells can switch from integrin-mediated to integrin-independent movement without any change in migration speed or directional persistence (10). Furthermore, integrin-mediated force coupling is not required for migration in constrained environments. The currently established notion is that integrins in immune cells act as a low-affinity frictional interface between cortical actin flow and the substrate, thereby facilitating cell locomotion (11–13).

In this study, we revisit this well-established notion, which, as our data on large traction forces generated by immune cells suggest, is not wrong but needs to be extended. We use human amniotic membrane (HAM) tissue as a tangible physiological model of interstitial tissue and track movements of NK92 cells using time-lapse confocal

Author contributions: T.C., A.L., C.V., B.F., and C.M. designed research; T.C., L.B., D.B., S.K., P.L.S., R.S., N.H., G.N., M.W., and S.B. performed research; T.C., S.K., P.L.S., R.S., N.H., A.W., R.G., E.W., M.S., M.W.B., G.N., M.W., and C.V. contributed new reagents/analytic tools; T.C., L.B., D.B., S.K., A.W., R.G., E.W., G.N., M.W., S.B., and C.M. analyzed data; M.S., M.W.B., and C.V. were responsible for handling patients and study consent; and T.C., P.L.S., R.S., B.F., and C.M. wrote the paper.

The authors declare no competing interest.

This article is a PNAS Direct Submission.

[1]To whom correspondence may be addressed. Email: christoph.mark@fau.de.

This article contains supporting information online at https://www.pnas.org/lookup/suppl/doi:10.1073/pnas.2524427123/-/DCSupplemental.

Published March 10, 2026.

microscopy (Movies S1–S3). In addition, we monitor tissue deformations around migrating NK92 cells using confocal reflection microscopy. Consistent with prevailing theories, our data confirm that immune cells appear to migrate in an ameboid manner within fibrous, collagen-rich HAM tissue most of the time, without significantly adhering to or pulling on their microenvironment. Interestingly and unexpectedly, this amoeboid migration mode is frequently interrupted by short phases during which the NK92 cells induce substantial and long-ranging matrix deformations along their axis of movement.

Since the local mechanical properties of HAM tissue around a migrating cell are difficult to measure, we further perform migration experiments using reconstituted collagen gels with well-defined mechanical and structural properties. This allows us to perform fast time-lapse 3D traction force microscopy to reconstruct cell-generated contractile forces, and to perform high-resolution bright-field microscopy to visually detect cell deformations due to steric hindrance during the passage of narrow pores in the matrix. We combine this technique with high-throughput 3D migration assays to relate cellular force generation to the migratory ability of immune cells under steric hindrance.

In previous work, Böhringer et al. (14) have shown that the amoeboid migration of NK92 cells embedded in 3D reconstituted collagen gels is frequently interrupted by short contractile bursts, with peak forces of up to ~60 nN. In this work, we test the hypothesis that during force bursts, immune cells switch to a highly contractile mesenchymal-like migration mode that allows them to overcome the steric hindrance imposed by narrow pores in the ECM and to avoid getting "stuck" in the matrix (Movies S4 and S5). We provide evidence for this hypothesis in four ways: first, we use high-resolution time-lapse microscopy to show that cell induced matrix deformations occur predominantly when the cell stalls during migration, before passing through a pore. Second, we find a significant temporal correlation between cell contractility, cell speed, and directional persistence of individual motile immune cells. Third, we find that by blocking integrin adhesion to the matrix, NK92 cells can still migrate in an amoeboid migration mode with unchanged migration speed, but the cells are forced to take more frequent turns to avoid small pores and obstacles, and become "stuck" more frequently (reduced motile fraction). Finally, we find that increasing the contractile forces of NK92 cells substantially increases the fraction of motile cells.

Results

Contractile Phases of NK92 Cells During Migration in HAM Tissue. The HAM makes up the inner layer of the placenta and can be dissected while remaining intact for further use (Fig. 1*A*). HAM is widely used as a scaffold for tissue engineering in regenerative medicine (15), or as a matrix to study cancer cell invasion (15, 16). With a shear modulus of 100-400 Pa, depending on preparation, HAM represents soft human tissue, which makes it an ideal system to detect cell-induced matrix deformations (17). HAM consists of the amniotic surface layer containing epithelial polygonal cells, a basement membrane, and a fibrous extracellular matrix layer enriched in proteins including collagen I, collagen III, collagen IV, laminin, and fibronectin (Fig. 1 *B–D*) (18). Confocal reflection microscopy reveals a highly heterogeneous, fibrous structure of the ECM layer with a high variability in pore size (Fig. 1*E*). To test the ability of immune cells to invade such a mechanically challenging environment, we prepare HAM samples with the epithelial layer flipped downward, and seed NK92 cells on top of the ECM layer. By employing time-lapse confocal imaging, we can track the movements of individual NK92 cells within the matrix, and at the same time track any matrix deformations due to traction forces that cells exert onto the matrix during 3D migration (Fig. 1 *F–I* and Movies S1–S3).

NK92 cells readily invade into the HAM tissue. They migrate predominantly without noticeable matrix deformations, in support of an amoeboid migration mode, but they occasionally switch into a different migration mode in which we observe substantial matrix deformations toward the cell center, predominantly along the direction of cell movement (Fig. 1 *F* and *G* and Movies S1–S3). Hence, the cells pull on the matrix in short contractile bursts that last only a few minutes. These bursts are frequently accompanied by a decrease in cell width, likely due to the cell moving through a narrow pore of the fiber network (Fig. 1*H*). Shortly after a contractile event, we typically observe an increase in migration speed (Fig. 1*I*).

NK Cell Contractility Correlates With Matrix Pore Passage. While HAM tissue serves as a physiologically relevant model for interstitial tissue, it does not allow us to translate the measured deformations caused by a cell into contractile forces, as we cannot quantify the local mechanical properties of the highly heterogeneous HAM tissue. Furthermore, the highly variable pore size of the HAM tissue (c.f. Fig. 1*E*) complicates the search for a relation between cell contractility and steric hindrance. We overcome these limitations by seeding NK92 cells into reconstituted collagen gels with known mechanical and structural properties.

With a shear modulus of ~100 Pa at a concentration of 0.6 mg/mL, ~300 Pa at 1.2 mg/mL, and ~1,200 Pa at 2.4 mg/mL, reconstituted collagen gels accurately recapitulate the stiffness of HAM tissue (14). If we approximate the Young's modulus as $E = G \cdot 2 \cdot (1 + \nu)$ with a Poisson ratio of $\nu = 0.25$, we obtain a stiffness range for the collagen gels between ~250 to 3,000 Pa, which covers the microelasticity of brain (400 Pa), liver (1,350 Pa), kidney (2,600 Pa), and fat tissue (3,000 Pa) (19). Due to the highly nonlinear strain-stiffening behavior of collagen, the matrix surrounding an actively pulling NK cell may locally stiffen by a factor of 5 (*SI Appendix*, Fig. S1). This widens the stiffness range that is sensed by the embedded immune cells, which then includes the microelasticity of lung (6,000 Pa) and muscle (12 kPa) tissue, covering a wide range of tissue stiffness on the cellular scale (19). The mean pore size of the reconstituted collagen gels is estimated to be 5.7 μm at a concentration of 0.6 mg/mL, 4.4 μm at 1.2 mg/mL, and 3.5 μm at 2.4 mg/mL (14). Since pore sizes follow a Rayleigh distribution (20), their SD equals approximately half of their mean value, thus limiting the structural variability of the gels in contrast to the heterogeneous HAM tissue.

To relate cell-induced force generation to steric hindrance, we first focus on exemplary high-resolution time-lapse image series of NK cells embedded in reconstituted collagen matrices. By visually identifying local impingements of the cell body, we identify steric constrictions in the matrix (Fig. 2 *A* and *E*). We then quantify the dwell time of the cell at different positions in the gel using image segmentation, and determine cell-induced matrix deformations via particle image velocimetry. Combining both information allows us to directly relate the positions of constricting pores within the gel with changes in cell tractions (Fig. 2 *B* and *F*). For an exemplary NK92 cell embedded in dense 2.4 mg/mL collagen, we find that the cell remains trapped for ~1 h as it probes the passage of multiple pores, before squeezing through a pore within only a few minutes (Fig. 2 *A* and *B* and Movies S6 and S7). We find smaller cell-induced matrix deformations pointing toward pores that the cell probed but did not traverse, and we find the largest matrix deformations pointing toward the pore that the cell traversed (Fig. 2*B*).

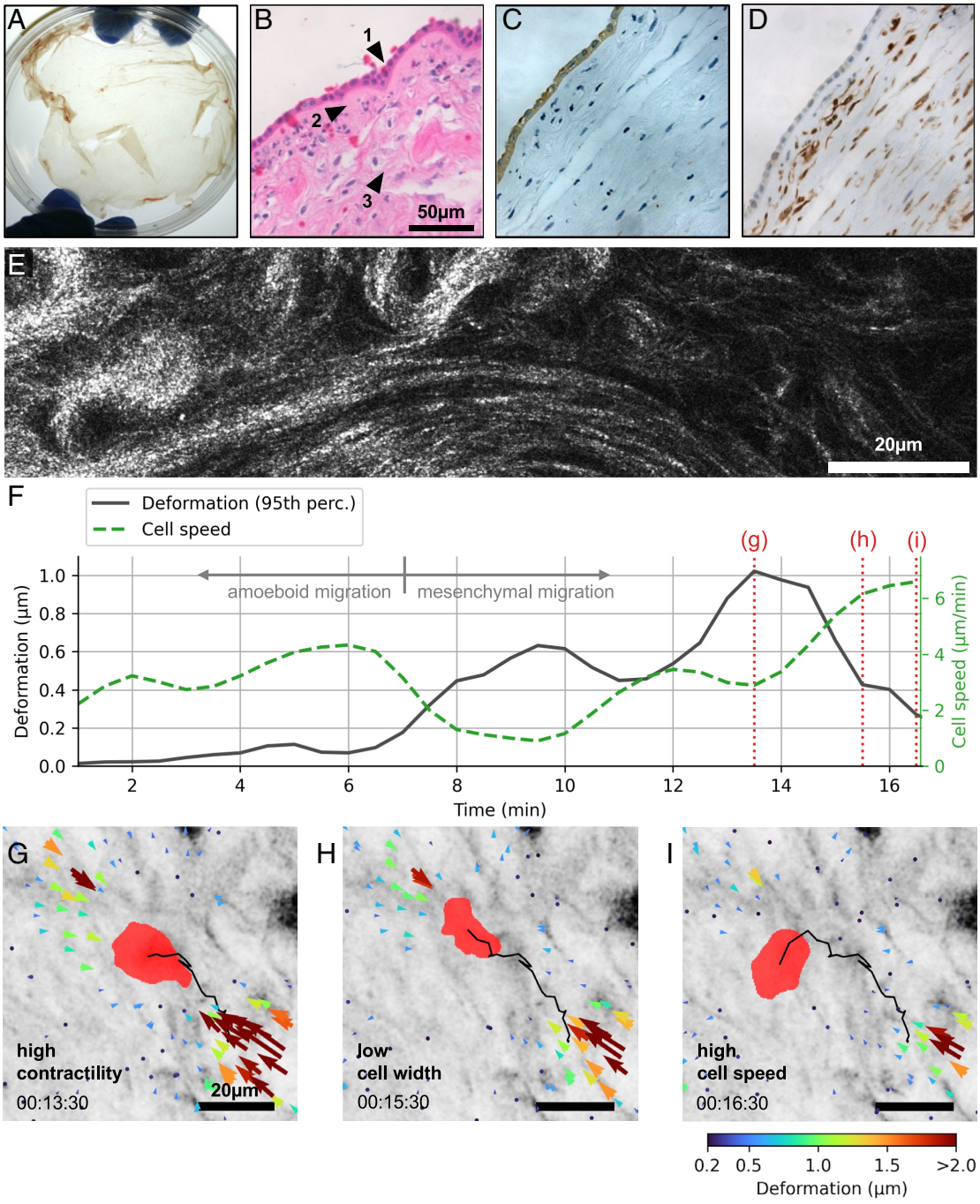

Fig. 1. Migration of NK92 cells in ex-vivo amniotic membrane tissue. (*A*) Macroscopic image of human amniotic membrane (HAM) tissue after fractionation from the placenta. (*B*) Cross-sectional H&E stain of a HAM sample, showing the epithelial layer 1), the basement membrane 2), and the fibrous extracellular matrix layer 3). (*C*) Cross-sectional pan-cytokeratin staining of a HAM sample, highlighting the epithelial layer (brown). (*D*) Cross-sectional vimentin staining of a HAM sample, indicating the presence of fibroblasts in the fibrous extracellular matrix layer (brown). (*E*) Exemplary confocal reflection image of a HAM sample showing the fibrous extracellular matrix layer and illustrating its structural heterogeneity, from thick, dense fiber bundles and small pore sizes on the *Left* to thinner fibrils and larger pore sizes on the *Right*. (*F*) Time course of the matrix deformations (black line) and migration speed (green dashed line) of an exemplary NK92 cell migrating in HAM tissue. We use the 95th percentile of all deformations within 100 µm around the cell to quantify highly localized deformations corresponding to contractile cell forces. Dotted red lines indicate the time steps corresponding to the deformation fields shown in panels (*G–I*). (*G*) Inverted collagen reflection image (gray) of an exemplary NK92 cell (red) migrating through HAM tissue. Arrows indicate strong contractile matrix deformations along the direction of cell movement (black line; c.f. panel *F*). (*H*) Same as in (*G*), but two minutes later, when the cell has reduced its width perpendicular to the direction of movement (presumably to pass through a narrow pore), while matrix deformations are partially relaxed (c.f. panel *F*). (*I*) Same as in (*H*), but one minute later, when matrix deformations are almost completely relaxed and the cell has attained a high migration speed again.

Since NK92 cells generally exhibit a larger cell size and a more spherical morphology compared to primary NK cells (*SI Appendix*, Fig. S7), we next investigated primary, blood-derived NK cells that are expanded for 14 d in the presence of high concentrations of IL-2 and IL-15-secreting feeder cells. Such ex-vivo expanded NK cells are currently explored for use in adoptive immunotherapy against blood-borne cancers (21, 22). They are highly motile in reconstituted collagen gels and feature a pronounced elongated shape during migration (Fig. 2*E*). Quantifying dwell time, matrix deformations, and constraining pores for an exemplary expanded NK cell embedded in a 1.2 mg/mL collagen gel, we find that the cell predominantly stalls in front of pores, and we find that

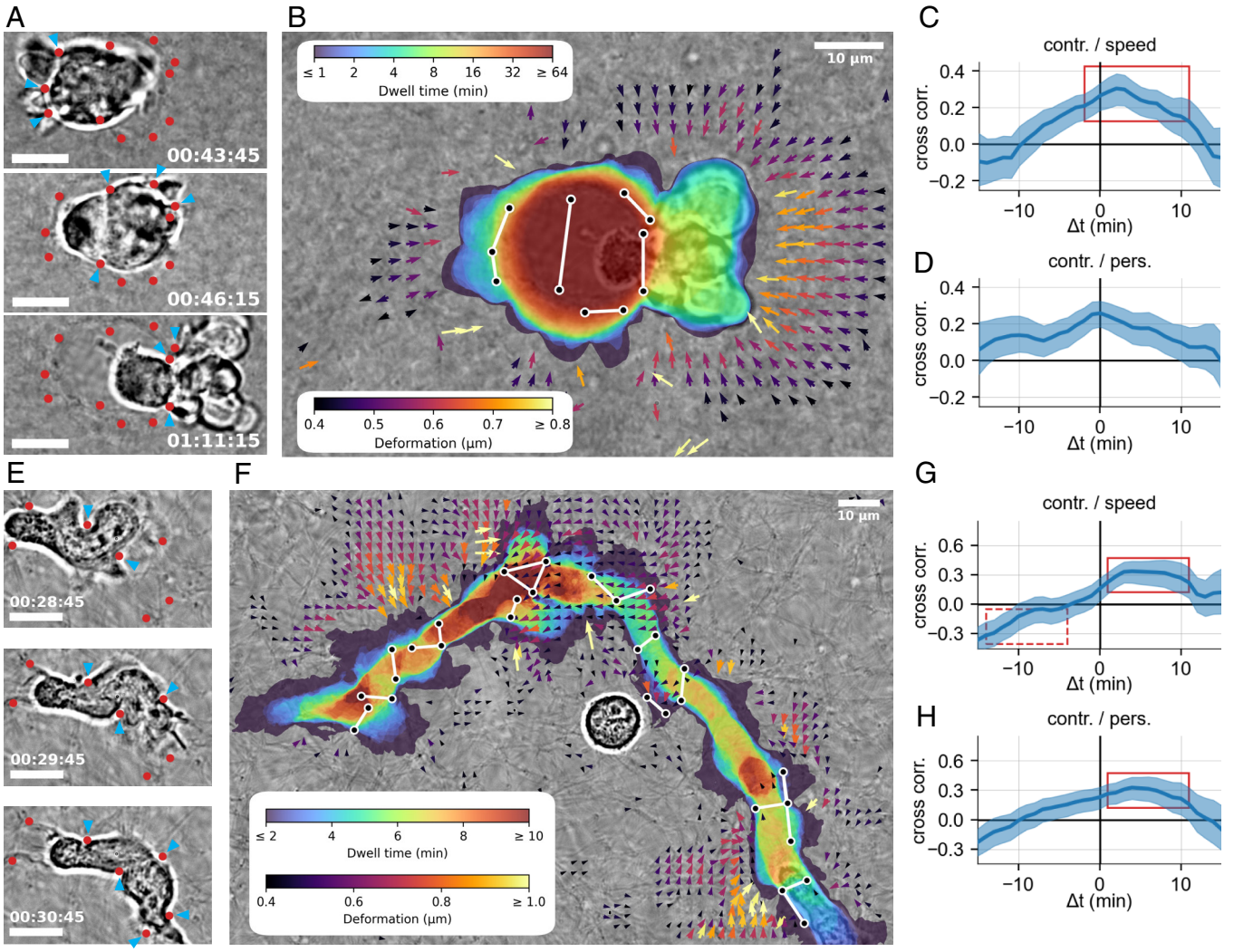

Fig. 2. Matrix pore passage regulates NK cell contractility. (*A*) High-resolution brightfield images of an exemplary NK92 cell embedded in a 2.4 mg/mL collagen matrix at different time points (*Top* to *Bottom*). Red points indicate matrix constrictions that are visually identified by impingements of the cell body. In each image, blue arrows indicate the matrix constrictions that currently act on the cell. (*B*) Overlay image showing an exemplary NK92 cell embedded in a 2.4 mg/mL collagen matrix. Color shading indicates the dwell time of the cell at different positions in the gel; dark blue areas denote regions that the cell only explored briefly for 1 min or less, dark red areas denote regions that the cell occupied for more than one hour. Matrix deformations as detected by particle image velocimetry are denoted by colored arrows. Matrix pores as identified by visible cell membrane indentations are denoted by white lines with black end-points. (*C*) Cross-correlation function between cell contractility and cell speed of NK92 cells embedded in 1.2 mg/mL collagen gel, as measured by 3D TFM. Positive x-values indicate that speed follows contractility in time, negative x-values indicate that contractility follows cell speed. The correlation function is based on data from n = 52 cells and considers all time steps with positive contractility. The red rectangle indicates the right-shifted peak of the correlation function. Error intervals indicate 1 SEM obtained by bootstrapping. (*D*) Same as in (*C*) but showing the cross-correlation function between contractility and directional persistence. (*E*) Same as in (*A*), but for an exemplary expanded NK cell embedded in 1.2 mg/mL collagen gel. (*F*) Same as in (*B*), but for an exemplary expanded NK cell embedded in 1.2 mg/mL collagen gel. (*G*) Cross-correlation function between cell contractility and cell speed of expanded NK cells embedded in 1.2 mg/mL collagen gel, as measured by 3D TFM. Positive x-values indicate that speed follows contractility in time, negative x-values indicate that contractility follows cell speed. The correlation function is based on data from n = 64 cells and considers all time steps with a positive contractility. The solid red rectangle indicates the right-shifted peak of the correlation function. The dashed red rectangle marks the negative correlation between contractility following cell speed. Error intervals indicate 1 SEM obtained by bootstrapping. (*H*) Same as in (*G*), but showing the cross-correlation function between contractility and directional persistence.

cell-induced matrix deformations are predominantly found pointing toward the pores that cause the cell to stall (Fig. 2*F* and Movies S8 and S9). While of exemplary nature, these findings clearly indicate that NK cells employ traction forces specifically when stalling during migration, which in turn happens predominantly when they encounter constricting pores.

To provide further evidence that NK cells use traction forces specifically to enhance their migration, we apply high-speed 3D traction force microscopy (TFM) (14). For 3D TFM, we quantify the 3D matrix deformations around individual NK92 and expanded NK cells embedded in 1.2 mg/mL collagen gels using particle image velocimetry applied to confocal reflection microscopy image stacks recorded over 24 min at a time interval of 1 min. We reconstruct the cell-generated forces responsible for the observed matrix deformations using high-speed 3D traction force microscopy, and subsequently sum up all force vectors that are directed toward the cell to obtain the contractility at each point in time (8, 14, 23).

Böhringer at al. (14) have previously reported that NK92 cell contractility increases with increasing matrix stiffness, reaching ~60 nN at the highest collagen concentration (2.4 mg/mL, corresponding to 1,155 Pa shear modulus). Given the small size of NK92 cells, this contractility is surprisingly high—comparable to mesenchymal cancer cells that generate forces of ~100 nN (8, 24). The even smaller ex-vivo expanded NK cells generate their maximal contractility of ~30 nN when embedded in a 1.2 mg/mL

collagen gel. By combining traction force microscopy and automated cell tracking, Böhringer at al. (14) have further identified a positive correlation between cell speed and contractility, indicating that NK92 cells use traction forces to speed up.

To confirm our exemplary findings that relate NK cell contractility to the passage of narrow pores, we refine and extend this correlation analysis. To this end, we track the position of individual cells during the 3D traction force microscopy measurement and extract the momentary cell speed and turning angle between subsequent time steps. As we are interested in the systematic movement of the cell as a whole, we employ Bayesian filtering to suppress spurious movements of the cell due to cell shape variations and imaging noise (*Materials and Methods* and *SI Appendix*, Fig. S2) (25, 26). Our hypothesis that NK cells use traction forces to overcome steric hindrance suggests a time-shifted peak in the cross-correlation functions between cell contractility and cell motility, as described below.

For NK92 cells, we find that, on average, cell speed increases after a burst in cell contractility, with a small time lag of 2 min, suggesting that NK92 cell motility benefits from contractile forces (Fig. 2 *C* and *D*). This interplay of cell motility and cell contractility is more pronounced in the ex-vivo expanded NK cells, for which phases of elevated contractility are followed by phases of elevated speed and persistence lasting for ~10 min (Fig. 2 *G* and *H*). Phases of elevated cell speed, by contrast, are followed by phases of reduced contractility lasting for ~15 min (Fig. 2*G*). Hence, the cell preferentially upregulates traction forces after it becomes slower or less persistent.

These dynamic patterns closely resemble the gliding motion during mesenchymal migration of breast cancer cells, but on a faster time scale. Cross-correlation functions fall to zero within 10 to 15 min for NK92 and expanded NK cells, compared to 1 h for MDA-MB-231 cells (8). This striking similarity in migration dynamics supports our hypothesis that NK cells are able to switch to a mesenchymal-like migration mode to maintain their motility in challenging microenvironments.

Inhibition of Acto-Myosin-Driven Forces Decreases the Motile Fraction of NK92 Cells. If NK cells use traction forces to overcome steric hindrance in 3D collagen gels, we expect that inhibition of cellular force generation will result in a lower motile fraction as more cells become "stuck" in the narrow pores of the gel. To test this hypothesis, we downregulate acto-myosin contraction in NK92 cells by treating the cells with Rho kinase inhibitor or with blebbistatin. We use concentrations that reduce the magnitude (Fig. 3*A*) and frequency of force peaks (Fig. 3*B*), but do not completely inhibit cellular force generation so that the cells retain their ability for dynamic shape changes and migration. In previous work, Böhringer at al. (14) have shown that this treatment significantly decreases the contractility and fraction of time that the cells are contractile (Fig. 3 *A* and *B*; reproduced from Ref. 14).

To relate the decrease in cell contractility to cell motility, we consider the motile phases of NK92 cells. We draw a bounding-box around a cell's migration path during each 5 min period and determine its diagonal length (a measure of the exploration volume). A cell is classified as motile if the diagonal is greater than 6.5 μm on average over the 24 min observation time. In agreement with our hypothesis, we find that the fraction of motile NK92 cells is substantially reduced by ~50% when acto-myosin contraction is reduced (Fig. 3*C*). Importantly, the treatment does not affect cell viability (*SI Appendix*, Fig. S3).

To validate this finding based on a larger cell population, we perform high-throughput 3D migration assays in which NK92 cells are seeded into a collagen matrix and then imaged and tracked

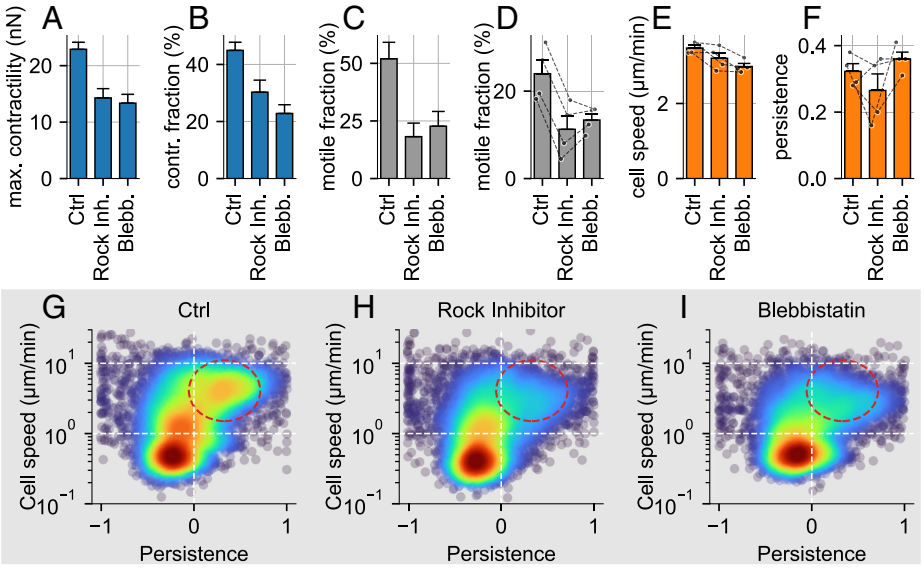

Fig. 3. Inhibition of acto-myosin-driven forces in NK92 cells decreases motile fraction, but not motility. (*A*) Cell contractility, evaluated by taking the mean over the maximum contractility of each cell during a 24 min observation period (to capture the contractility during the short contractile bursts that NK92 cells exhibit), for the control and for treatment with 10 μM Y-27632 Rock-inhibitor and 3 μM blebbistatin in a 1.2 mg/mL collagen gel (Ctrl n = 50, blebbistatin n = 44, Rock inhibitor n = 44 cells) in 3 independent experiments [data from Böhringer et al. (14)]. (*B*) Contractile fraction of the NK92 cells, calculated as the average fraction of time steps that the cells reach a contractility >5 nN. (*C*) Fraction of motile NK92 cells. A cell is motile if the 5 min bounding-box around its migration path has a mean diagonal length of 6.5 μm or greater. (*D*) Same as in (*C*), but measured in the high-throughput 3D migration assay (n = 3 independent experiments, n = 1,000 to 3,500 cells per measurement and condition, one tailed paired *t* test, $P < 0.0001$ for Rock inhibitor, $P = 0.0051$ for blebbistatin). (*E*) Mean speed of motile NK92 cells as measured in the high-throughput 3D migration assay, paired for all three conditions. Individual paired measurements are indicated by the black dots and lines (n = 4 independent experiments; 1,000 to 3,500 cells are measured per measurement and condition). (*F*) Same as in (*E*) but showing the mean directional persistence of motile NK92 cells. (*G*) Density plot of cell speed and persistence under control conditions. Each point represents the mean cell speed and persistence of a 5 min trajectory of a single NK92 cell. The color shading represents the Gaussian kernel density estimate (n = 4 independent experiments). Red dashed circle approximately indicates the motile fraction of the cell population that migrates at least 6.5 μm from its point of origin within 5 min. (*H*) Same as in (*G*), but for NK92 cells treated with 10 μM Y-27632 Rock-inhibitor. (*I*) Same as in (*G*), but for NK92 cells treated with 3 μM blebbistatin.

at low magnification for 5 min in multiple field-of-views. This technique allows us to acquire data on 1,000 to 3,500 individual cells per condition and experiment. We perform this additional assay for two reasons: first, there may be a selection bias toward elongated, motile cells in single cell 3D TFM measurements, as the investigator must manually search for and select cells for imaging. Second, the high-throughput 3D migration assay allows us to perform paired experiments for all conditions and obtain data on a much larger population of cells.

The high-throughput migration assay shows a lower motile fraction under all conditions compared to the 3D TFM experiment (Fig. 3*D*), confirming a selection bias toward motile cells in the single-cell 3D TFM experiment. However, the 50% decrease in the motile fraction after downregulation of acto-myosin contraction remains and is consistently observed in all independent replicates of the experiment (Fig. 3 *D* and *G–I*). Interestingly, cells that remain motile after treatment suffer only a small ~10% decrease in cell speed (Fig. 3*E*), and no change in directional persistence (Fig. 3*F*).

Acto-myosin activity not only facilitates the exertion of pulling forces on the ECM but also drives cell shape changes via the actin cortex during amoeboid migration. To separate both mechanisms, we place the cells in nonadhesive carbomer gels, thereby forcing them into an amoeboid migration mode. As expected, we find that without adhesion to the ECM, the motile fraction in carbomer is generally lower than in collagen, but we further find that the reduction of acto-myosin contraction after Rho kinase inhibition and blebbistatin treatment has a less pronounced effect of only 20 to 25% on the motile fraction in carbomer, compared to 50% in collagen (*SI Appendix*, Fig. S4). This confirms that the decrease of the motile fraction in collagen after partial acto-myosin inhibition is to a large degree attributable to the inhibition of cell-generated traction forces.

These findings provide two main insights: first, the motile fraction is a sensitive metric to quantify the migratory ability of NK cells. Second, these results confirm that large cell tractions are critical for overcoming the steric hindrance when encountering narrow pores, but are much less critical for amoeboid motion in less challenging environments.

Contractile Forces of Primary Immune Cells. The observation of short contractile phases is not limited to the cultured NK92 cell line. Rather, we find that most immune cell types are capable of generating appreciable traction forces. In particular, we find that without expansion, primary human B cells, monocytes, NK cells, T cells, and neutrophils all exhibit contractile phases on the order of ~5 nN (with occasional peaks around 20 nN) in which they spend 5-10% of the time when placed in a 1.2 mg/mL collagen matrix with a low stiffness of 85 Pa (Fig. 4 *A* and *B*). We further confirm that traction forces facilitate migration of primary cells, as cell speed and directional persistence increase after force upregulation (*SI Appendix*, Fig. S5). For all cell types, the fraction of motile cells remains lower compared to NK92 cells and is subject to significant donor-to-donor variation (Fig. 4*C*).

Over a time course of 24 h, B cells increase the frequency of contractile bursts and also increase their motile fraction, whereas monocytes decrease the frequency of contractile bursts and also decrease their motile fraction (Fig. 4 *B* and *C*). We find a positive correlation between the 24 h change in burst frequency and the change in motile fractions among different cell types (Fig. 4*D*), highlighting the importance of contractile force bursts in the 3D migration process for a diverse set of primary immune cells.

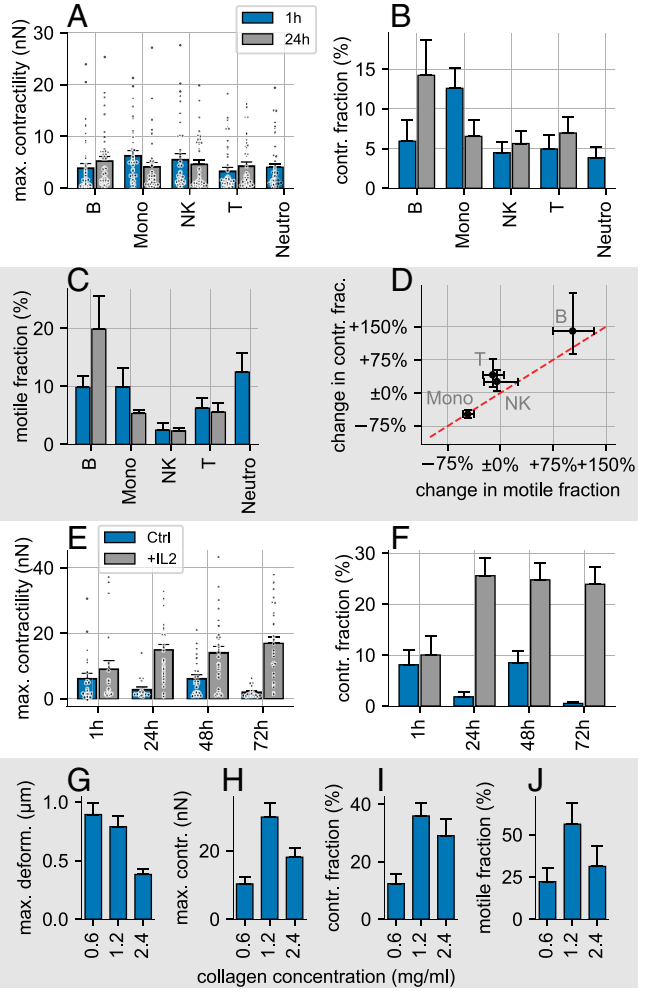

Fig. 4. Traction forces of primary immune cells. (*A*) Cell contractility, evaluated by taking the mean over the maximum contractility of each cell during the 24 min observation period (to capture the contractility during the short contractile bursts) for different primary immune cells 1 h (blue) and 24 h (gray) after seeding the cells into the 3D collagen gels (B-cells: "B," n = 43/44; Monocytes: "Mono," n = 39/44; Neutrophils: "Neutro," n = 47/0; NK cells: "NK," n = 41/43; T cells: "T," n = 48/43 in 4 independent experiments). Each black dot represents the maximum contractility of an individual cell. (*B*) Contractile fraction of different primary immune cells, calculated as the average fraction of time steps that the cells reach a contractility >5nN. (*C*) Fraction of motile primary immune cells as measured in the high-throughput migration assay. (*D*) Change in the mean fraction of time steps with a contractility >5nN (called "contractile fraction") within the first 24 h after seeding the cells into the collagen gel, as a function of the change in the motile fraction of the cell population (as measured in the migration assay). The red dashed line indicates the identity line. (*E*) Cell contractility of primary NK cells after incubation with IL-2 (gray) and without (control; blue), for different incubation periods prior to seeding the cells into the collagen gel. Each black dot represents the maximum contractility of an individual cell. (*F*) Contractile fraction of primary NK cells after incubation with IL-2 (gray) and without (control; blue), for different incubation periods prior to seeding the cells into the collagen gel. (*G*) 99th percentile of the matrix deformations generated by ex-vivo expanded NK cells for different collagen concentrations (0.6 mg/ml: n = 27; 1.2 mg/mL: n = 16; 2.4 mg/mL: n = 16 in 2 independent experiments). (*H*) Maximum cell contractility during a 24 min observation period. (*I*) Fraction of contractile phases (time periods when cell contractility > 5 nN). (*J*) Fraction of motile expanded NK cells for different collagen concentrations. Error bars denote 1 SEM in (*A–C*) and (*E–J*), and the 1-sigma credible interval obtained by bootstrapping in (*D*).

Migration and Contractile Forces of Ex Vivo Expanded NK Cells. The low contractility of the primary cells compared to NK92 cells noted above is due to the fact that these cells have not been specifically activated before the TFM measurements. Since IL-2 activation is known to promote cell motility (27), we reasoned

that this effect might be supported by an increased contractility. We confirm that the motile fraction of primary NK cells without IL-2 decreases over a 72 h time period, but remains high when stimulated with IL-2 (*SI Appendix*, Fig. S6). Similarly, the magnitude and frequency of contractile bursts increase within 1 h after IL-2 addition and remain stable for the following 72 h, whereas contractile forces decline toward zero over this time period in nonstimulated cells (Fig. 4 *E* and *F*). These data suggest that the enhanced migration of NK cells after IL-2 activation is indeed facilitated by increased cellular force generation.

To relate these findings to a clinical translational setting, we next investigated NK cells that are expanded for 14 d in the presence of high concentrations of IL-2 and IL-15-secreting feeder cells, resulting in a population of highly activated NK-cells that are currently explored for use in adoptive immunotherapy (21, 22). In general, we find that expanded NK-cells are similarly motile and contractile as IL-2 stimulated primary cells and NK92 cells (c.f. Fig. 3 *A* and *B*). Moreover, cell-induced matrix deformations show a monotonic decrease with collagen concentration, similar to the results for NK92 cells (14).

However, we find some notable qualitative differences. While Böhringer at al. (14) have reported that the reconstructed contractility of NK92 cells increases monotonically with collagen concentration (and thus with matrix stiffness), the maximum contractile force and the contractile fraction of expanded NK cells show a pronounced biphasic response to collagen concentration, reaching the highest values at an intermediate (1.2 mg/mL) collagen concentration (Fig. 4 *H* and *I*). This qualitative difference is likely a result of the smaller size of the expanded NK cells compared to NK92 cells (*SI Appendix*, Fig. S7) and illustrates that cell motility depends on a combination of matrix stiffness, pore size relative to cell size, and traction forces. This notion is furthermore supported by our finding that the motile fraction of ex-vivo expanded NK cells is roughly proportional to the magnitude and frequency of force bursts (Fig. 4 *H–J*).

3D NK Cell Motility Depends on Cell–matrix Adhesion. The reduced motile fraction of NK cells after force inhibition, and the correlation between contractility and cell speed, provide strong but indirect evidence for our hypothesis that immune cells use traction forces to overcome steric hindrance during 3D migration. Traction forces require strong adhesion to the matrix (28, 29). If NK cells use adhesion-mediated traction forces only when confronted with steric hindrance, we predict that any down-regulation of cell–matrix adhesion will result in a reduced motile fraction (more cells become "stuck") and a reduced directional persistence (cells take more turns to avoid obstacles). However, we do not expect cell speed to be significantly affected, as motile cells should still be able to migrate in a nonadhesive, amoeboid fashion as long as they do not encounter narrow pores within the matrix.

To test this hypothesis, we modulate cell–matrix adhesion by changing either matrix adhesiveness and/or the ability of the cells to form adhesions. First, we add the adhesion-inhibiting surfactant pluronic to polymerized collagen gels to reduce direct contacts between the cell membrane and individual collagen fibers, forcing the NK cells into a nonadhesive migration mode (30). For NK92 cells, pluronic treatment reduces the fraction of motile cells by ~25% and the directional persistence of the remaining motile cells also by ~25% (Fig. 5*A* and *SI Appendix*, Fig. S3). Consistent with our hypothesis, the remaining motile cells maintain their full migratory speed (Fig. 5*A*). Second, we seed NK92 cells into nonadhesive colloidal carbomer gels (Fig. 5*B*). These gels are composed of cross-linked polymer particles and provide a soft elasto-plastic microenvironment (24, 31, 32) (*SI Appendix*, Fig. S8 and Movie S10). The relative

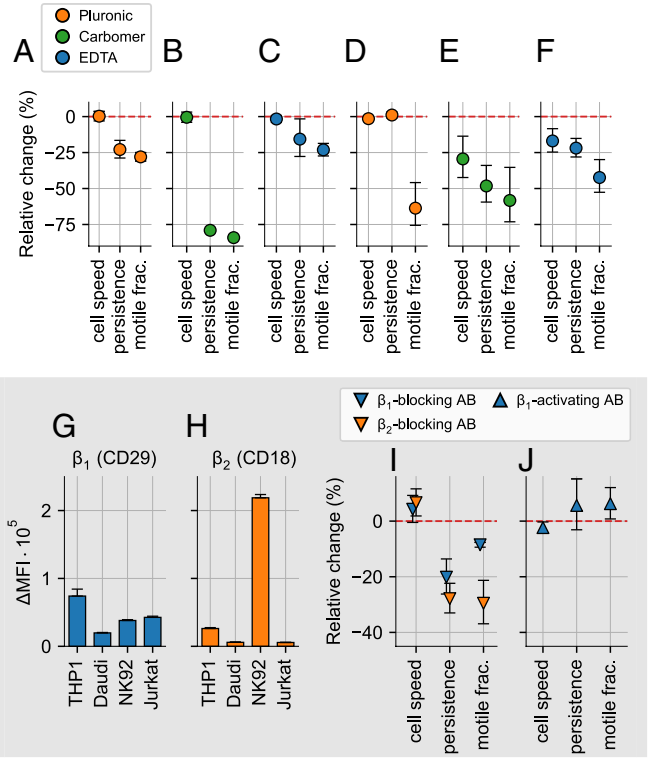

Fig. 5. Inhibiting cell–matrix adhesion suppresses NK cell motility. (*A*) Relative change of cell speed, persistence, and motile fraction of NK92 cells, measured in high-throughput 3D migration assays (n = 3 independent experiments) after inhibiting cell–matrix adhesion externally by the addition of pluronic to collagen gels (hindering cells from making contact with collagen fibers; orange; $P = 0.02$ for the motile fraction, $P = 0.94$ for cell speed, $P = 0.08$ for persistence). (*B*) Same as in (*A*), but for NK92 cells in nonadhesive carbomer gels (n = 3; green; $P < 0.001$ for the motile fraction, $P = 0.90$ for cell speed, $P = 0.001$ for persistence). (*C*) Same as in (*A*), but for EDTA-treated NK92 cells in collagen (n = 3; blue; $P = 0.04$ for the motile fraction, $P = 0.56$ for cell speed, $P = 0.38$ for persistence), limiting cell–matrix adhesion internally by removing calcium ions that integrins require to maintain adhesion to the matrix. (*D*) Same as in (*A*), but for ex-vivo expanded NK cells (n = 2, $P = 0.24$ for the motile fraction, $P = 0.19$ for cell speed, $P = 0.69$ for persistence). (*E*) Same as in (*B*), but for ex-vivo expanded NK cells (n = 8, $P = 0.09$ for the motile fraction, $P = 0.13$ for cell speed, $P = 0.03$ for persistence). (*F*) Same as in (*C*), but for ex-vivo expanded NK cells (n = 7, $P = 0.03$ for the motile fraction, $P = 0.11$ for cell speed, $P = 0.03$ for persistence). (*G*) Delta mean fluorescence intensity of CD29 (β1 integrin) of immune cell lines (THP1, Daudi, NK92, and Jurkat cells), measured by flow cytometry (n = 3). (*H*) Same as in (*G*), but for CD18 (β2 integrin) (n = 3). (*I*) Same as in (*A*), but for treatment of NK92 cells with a β1 blocking antibody (blue; $P = 0.01$ for the motile fraction, $P = 0.46$ for cell speed, $P = 0.10$ for persistence) and a β2 blocking antibody (orange; $P = 0.05$ for the motile fraction, $P = 0.26$ for cell speed, $P = 0.02$ for persistence) in collagen (n = 3). (*J*) Same as in (*I*), but for β1 (blue) activating antibody treated cells in collagen (n = 3; $P = 0.37$ for the motile fraction, $P = 0.37$ for cell speed, $P = 0.59$ for persistence). Statistical significance is tested using a paired ratio *t* test.

changes in NK92 cell migration in carbomer gels confirm the results obtained under pluronic treatment, but show a much more pronounced decrease in the motile fraction and directional persistence of motile cells by >75% (Fig. 5*B*). Strikingly, the migration speed of the remaining motile cells remains unchanged (Fig. 5*B*).

We next test how NK cell migration changes when cells are treated with the calcium chelator EDTA. EDTA binds calcium and magnesium ions that are required for the proper function of several adhesion proteins, including integrins (33). For EDTA-treated NK92 cells in collagen gels, we find that the motile fraction is reduced by ~25%, the directional persistence of the remaining motile cells is reduced to a lesser extent, and the migration speed of the remaining motile cells is not affected (Fig. 5*C*). While the effects of pluronic, carbomer, and EDTA on cell migration differ on a quantitative level, they show a similar qualitative pattern: fewer cells

remain motile, and the remaining motile cells have to make additional turns within their microenvironment.

For ex-vivo expanded NK cells, the response after manipulation of cell–matrix adhesions is more nuanced. Pluronic treatment results in a large reduction of the motile fraction by >50%, but the remaining motile cells retain their migration speed and directional persistence (Fig. 5*D*). In carbomer gels and after EDTA treatment, ex-vivo expanded NK cells respond similar to NK92 cells, with a large decrease in motile fraction, a less pronounced decrease in directional persistence, and a smaller decrease in cell speed (Fig. 5 *E* and *F*). The difference between NK92 cells and ex-vivo expanded NK cells may be attributed to the smaller size of ex-vivo expanded NK cells with respect to pore size and spacing between obstacles in the matrix (*SI Appendix*, Figs. S7 and S8).

Pluronic, carbomer, and EDTA broadly inhibit cell adhesion to the matrix without specificity for particular adhesion molecules. Since the dynamic force regulation of NK cells is reminiscent of mesenchymal cells, we further hypothesize that force transmission to the ECM in NK cells is integrin-mediated. To test this hypothesis, we treat NK92 cells with antibodies that specifically block or activate β_1 and β_2 integrin subunits. Integrin β_1 (CD29) is expressed on many cultured immune cell lines, including THP1 monocytic cells, Daudi B cells, the NK92 cell line, and Jurkat T cells (Fig. 5*G*). Integrin β_2 (CD18) shows a fivefold higher expression level in NK92 cells compared to integrin β_1. The expression of β_2 is at least eightfold higher in NK92 cells compared to the other tested immune cell lines (Fig. 5*H*). Therefore, we expect that NK92 cells mainly rely on integrin β_2 for adhesion (34), and that blocking integrin β_2 will affect the motile fraction more than blocking integrin β_1. Indeed, 3D migration assays confirm that blocking integrin β_1 decreases the motile fraction of NK92 cells by ~10%, whereas blocking integrin β_2 results in a decrease of ~30% (Fig. 5*I* and *SI Appendix*, Fig. S3). Similar to our experiments in which adhesion is blocked in a nonspecific manner, we again find that directional persistence is significantly lower after integrin blocking. Notably, we find that cell speed is slightly increased after blocking β-integrins, likely because any type of integrin-mediated adhesion slows cells during their default amoeboid migration.

Treatment of NK92 cells with an activating integrin β_1 antibody leaves cell motility unchanged across all parameters (Fig. 5*J*). While we see a small increase in directional persistence and motile fraction, these changes are not statistically significant. This additional finding shows that NK cell motility is not a linear function of integrin activation, but that integrin activity is likely tightly regulated to achieve optimal motility in challenging microenvironments (13). In summary, manipulation of NK cell adhesion to the ECM demonstrates that NK cells generally achieve rapid migration in 3D biopolymer networks independent of adhesion to the ECM, but are critically dependent on adhesion to maintain motility and directional persistence in the presence of steric hindrance.

Disruption of the Microtubule Network Increases Traction Forces and Motile Fraction. Recent reports have demonstrated that the migration of T cells and their engagement with target cells can be improved by treatment with nocodazole (35, 36). Nocodazole inhibits the polymerization of tubulin and thus destabilizes the microtubule network in cells. Microtubule destabilization has two effects: first, the nuclear deformability is increased (35), and second, acto-myosin contraction is increased (36, 37). The current understanding is that enhanced immune cell migration under nocodazole treatment is achieved by an increased nuclear deformability as it eases the transition of the cell through narrow pores (2, 35), and by increasing cortical contraction and thus facilitating a fast, contact-guided, amoeboid migration mode in "2.5D" nano-structured surfaces (36). Here, we provide further context on the effect of nocodazole by investigating cellular force generation and migration of NK92 cells under treatment in 3D collagen gels.

We find that nocodazole treatment substantially increases traction forces of NK92 cells by more than 100% (Fig. 6*A*). Moreover, treated cells employ traction forces greater than 5 nN more often, in more than 30% of all measured time steps, compared to 15% for untreated cells (Fig. 6*B*). In accordance with our hypothesis that traction forces help cells to overcome steric hindrance, we find that nocodazole treatment of NK92 cells significantly increases the fraction of motile cells (Fig. 6*C*). Strikingly, we again see that cell speed of the motile cells is not affected by treatment (Fig. 6*D*), indicating once more that traction forces do not make cells faster, but instead prevent them from becoming "stuck". Directional persistence is significantly increased after nocodazole treatment (Fig. 6*E*), further underlining that higher traction forces alleviate the need to take turns to avoid obstacles within the ECM.

Finally, we investigate the effect of an initial nocodazole treatment of NK92 cells on their long-term migration behavior. We find that the initial, strong increase in the motile fraction and in persistence has a short lifetime of < 6 h (Fig. 6*F*). Importantly, after 18 h measurement time, the majority of all treated cells have

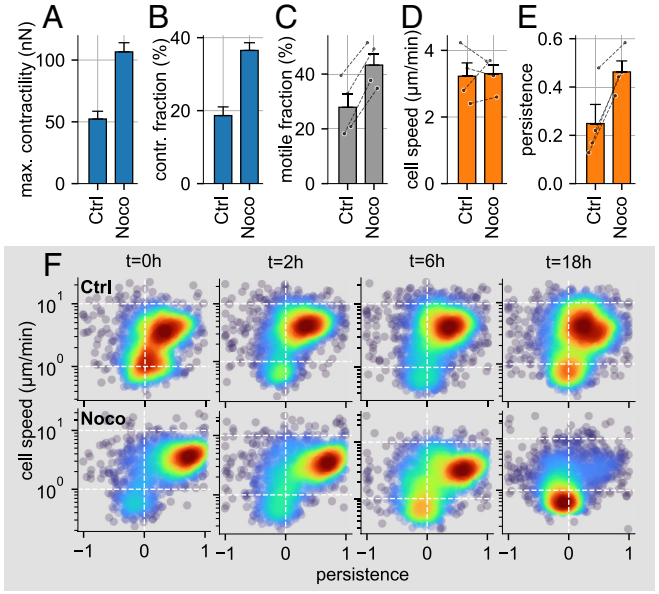

Fig. 6. Disruption of microtubule network in NK92 cells increases traction forces and motile fraction. (*A*) Maximum cell contractility of NK92 cells during a 24 min observation period for the control and for treatment with 10 µM nocodazole (control: "Ctrl" n = 46; nocodazole: "Noco" n = 49 cells) in 1.2 mg/mL collagen in 4 independent experiments. (*B*) Contractile fraction of the NK92 cells, calculated as the average fraction of time steps that the cells reach a contractility >5 nN. (*C*) Fraction of motile NK92 cells measured in the high-throughput 3D migration assay, paired for both conditions. Individual paired measurements are indicated by the black dots and lines (n = 4 independent experiments; 3000-4000 cells are measured per measurement and condition, one tailed paired *t* test, *P* = 0.001). (*D*) Same as in (*C*) but showing the mean speed of motile NK92 cells (one tailed paired *t* test, p = 0.409). (*E*) Same as in (*D*) but showing the mean directional persistence of motile NK92 cells (one tailed paired *t* test, *P* = 0.005). (*F*) Density plot of cell speed and persistence for NK92 cells under control conditions (*Top* row) or for NK92 cells treated with 10 µM nocodazole (*Bottom* row), for different measurement times (0 to 18 h) after seeding untreated and treated NK92 cells in collagen. Each point represents the mean cell speed and persistence of a 5 min trajectory of a single NK92 cell. The color shading represents the Gaussian kernel density estimate (n = 1 independent experiments, 1,500 to 2,000 cells are measured per condition for each measurement time).

become nonmotile, whereas the motile fraction of the control cells remains stable (Fig. 6*F*). The short-term positive effect of nocodazole on NK cell migration thus reverts on longer time scales, leaving most cells in a nonmotile state.

Discussion

We demonstrate that NK cells are capable of exerting significant traction forces on the ECM (in both ex-vivo HAM tissue samples and in-vitro 3D reconstituted collagen networks) that are comparable to the forces exerted by motile mesenchymal cells after accounting for the smaller size of immune cells. While we confirm the prevailing understanding that immune cells migrate in an amoeboid or friction-mediated manner without significant traction forces (4, 12), we find that immune cells temporarily switch to a highly contractile migratory mode during 10-20% (NK92 cells) (14) and 10 to 40% (expanded NK cells) of the total measurement time. Importantly, we show that cell-induced matrix deformations occur predominantly in the vicinity of matrix constrictions that impair cell migration.

Switching between the default, amoeboid migration mode and a more mesenchymal-like migration mode has previously been described in T cells after inhibition of Myosin-IIA, which induces a slower "sliding" migration mode with a continuously progressing contact zone on a 2D substrate (38). 2D traction forces have been measured in neutrophils (39) and T cells (40). Furthermore, leukocytes migrating in dense matrices repolarize into a mesenchymal configuration, placing the nucleus behind the centrosome (41). Our study complements these findings by measuring pulling forces of immune cells in 3D matrices and, importantly, linking the application of pulling forces to the ability of immune cells to overcome the steric hindrance of a 3D matrix.

To relate cellular force generation to cell motility in 3D, we have shown that both the migration speed and the directional persistence of individual NK cells increase dynamically during and after short contractile bursts. This supports our hypothesis that the switch from an amoeboid to a contractile migration mode is triggered when the cell encounters increased steric hindrance, similar to integrin-driven extravasation of immune cells. This synchronization of cell contractility, persistence, and cell speed is reminiscent of mesenchymal migration of motile cancer cells, which also rely on traction forces to overcome steric hindrance in 3D fiber networks (8, 9).

In support of the hypothesis that immune cells use traction forces to overcome steric hindrance, we further show that inhibition of the acto-myosin contraction in NK92 cells dramatically reduces both contractility and the fraction of motile cells, but has little effect on the migration speed and directional persistence of the remaining motile cells. These results suggest that unless a cell experiences steric hindrance (for example, by migrating through a narrow pore), it retains its default exploratory behavior and amoeboid migration mode. However, with limited acto-myosin contraction, cells are more likely to become "stuck", resulting in a significantly reduced motile fraction.

The combination of amoeboid migration and occasional contractile bursts is not specific to NK cells. Nonactivated primary B, T, and NK cells, as well as monocytes and neutrophils, are all able to exert traction forces on the ECM, although less frequently and not as strong as NK92 cells or expanded ex-vivo NK cells. Interestingly, cellular force generation appears to be closely linked to the adaptation process that immune cells undergo after being seeded into a 3D collagen matrix. Immune cell types that adapt well and increase their motile fraction over 24 h after seeding also increase the frequency of force bursts, and vice versa. Upon activation with IL-2, primary NK cells increase both the frequency and magnitude of force bursts. Thus, traction force generation may be a key determinant of immune cell infiltration and retention in mechanically challenging environments. Investigating to what extent different immune cell subtypes use traction forces in their respective homing tissues in-vivo would require very stable intravital imaging to detect small matrix deformations in the range of tens of nanometers. This is currently unfeasible, but future improvements may enable a direct verification.

Because large traction forces require a sufficiently strong coupling of the cell's contractile machinery to the extracellular matrix, it follows that immune cell migration in 3D biopolymer networks depends on cell–matrix adhesion. We have used several methods to inhibit cell adhesion to the ECM. In a nonadhesive environment, which can be achieved either by making collagen fibers nonadhesive using pluronic, or by seeding cells in nonadhesive carbomer gels, we find that the speed of NK92 cells is unchanged, but more cells become "stuck", and the remaining motile cells take more turns within the matrix. Treating cells with EDTA to weaken adhesion in a nonspecific manner confirms these findings. These effects are qualitatively replicated in ex-vivo expanded NK cells. In addition, we have shown that the migration of NK92 cells in 3D fiber networks depends on integrin-mediated adhesion to the matrix. Specifically, we find that blocking integrin β_1 and β_2 results in a substantial decrease in directional persistence and motile fraction, while cell speed is not reduced. Importantly, the decrease in motile fraction is greater when integrin β_2 is blocked compared to β_1, consistent with the higher expression level of β_2 in NK92 cells.

Finally, we have shown that nocodazole-induced depolymerization of microtubules in NK92 cells results in a substantial, temporary increase in traction forces, motile fraction, and directional persistence, while leaving cell speed of the motile cells unchanged. These results confirm a previously reported increase of the average cell speed under treatment (35, 36), but provide a more nuanced interpretation: not the cell speed of the motile cells changes under treatment, but the fraction of motile cells increases. Hence, nocodazole treatment does not make cells faster but prevents them from getting stuck. Our results suggest that apart from the previously reported increased nuclear deformation (2, 35), traction forces play a crucial role in the nocodazole-induced enhancement of migration.

These in-vitro experiments have implications for current cancer therapies: taxane-based chemotherapies stabilize microtubules to interfere with cell division, but they may further impair tissue- and tumor-infiltration by immune cells (36). Different chemotherapy agents, such as vinblastine, instead interfere with cell division by destabilizing microtubules, and may thus further enhance immune cell migration (35), at least on short time-scales. Functional biophysical assays that quantify migration behavior and mechanical interactions between cells and the ECM thus may help to better understand side effects and synergetic effects of existing anticancer therapies on immune cell behavior.

In conclusion, this investigation shows that immune cells are able to switch to a mesenchymal-like mode during 3D migration in physiological HAM tissue as well as in reconstituted biopolymer networks. This mesenchymal-like migration mode is characterized by integrin-mediated adhesion to the matrix and large, intermittent traction forces that the cells use to overcome steric hindrance.

Materials and Methods

Human Placenta Amniotic Membrane Isolation. Intact sterile placentae with chorion and amnionic membranes were collected from caesarian sections with informed consent for research use from all mothers. Whole placentae are washed at least five times to remove remaining blood. The HAM tissue is then dissected from the chorion layer using sterile forceps and placed in 60 mm tissue culture

dishes (*SI Appendix, Methods*) For tissue staining, HAM tissue samples are fixed with formalin and embedded in paraffin, then stained with hematoxylin eosin (Thermo-Fisher) or processed for immunohistochemistry (*SI Appendix, Methods*).

HAM Sample Preparation and Imaging. To prepare HAM samples for confocal imaging, we carefully cut a 5x5 mm piece using a scalpel, and position the ECM-side upward in the center of a Gene Frame (Thermo Fisher Scientific, cat. no. AB-0576) mounted on a 22 × 22 mm coverslip (Roth, cat. no. HKE7.1). We then add 20 μl of RPMI containing 120,000 NK92 cells stained for 20 min with calcein (2 μM, AAT Bioquest, cat. no. 22004) onto the HAM sample, and seal the frame with a second 22 × 22 mm coverslip. Every 30 s, we image a single z-plane around individual NK92 cells that have invaded into the ECM layer of the HAM sample using confocal microscopy (Leica DM 6000 CFS with HCX APO L 20×/1,00NA W objective). The sample is kept at 37 °C during the measurement. CO_2 content is not controlled as the samples are sealed.

NK92, Jurkat, Daudi, and THP1 Cell Lines. NK92 cells (purchased from ATCC CRL-2407) are cultured for 3 wk prior to measurements in Alpha-MEM medium (Stemcell Technologies) with 15% fetal calf serum (Sigma), 15% horse serum (Gibco), 500 IU/mL human interleukin-2 (IL-2) cytokine (Proleukin S, Aldesleukin, Novartis Pharma, cat. no. 02238131) and 1% penicillin-streptomycin solution (10,000 Units/mL Penicillin, 10,000 μg/mL Streptomycin, Gibco). Jurkat cells (gift from Prof. A. Baur, Department of Molecular Dermatology and Extracellular Vesicle Analysis, Erlangen, Germany), THP1 cells (gift from F. Rico, Aix-Marseille Université, CNRS, Inserm, LAI, Turing center for living systems), and Daudi cells (gift from A. Lux, Department of Genetics, Erlangen, Germany) are cultured for 3 wk prior to measurements in RPMI 1640 medium (Gibco) with 10% fetal calf serum, 1% Natrium Pyruvate (Gibco), 1% 100× MEM NEAA (Gibco), 0.3% 1 M HEPES (Gibco), and 1% penicillin-streptomycin solution (hereafter called R10 medium). Integrin expression profiles are determined by flow cytometry (*SI Appendix, Methods*).

Human Primary Immune Cell Isolation and Storage. Human peripheral blood is collected from healthy donors (Department of Transfusion Medicine and Hemostaseology, University Clinics Erlangen, Germany), with approved consent of all participants. The study was approved by the ethics committee of the Friedrich-Alexander University Erlangen-Nürnberg (22-320-Bp). Immune cells are isolated by density gradient centrifugation using Pancoll centrifugation media (PAN-Biotech, Aidenbach, Germany). Monocytes, NK cells, B cells, and T cells are extracted from the peripheral blood mononuclear cell (PBMC) layer (second layer) with negative magnetic-activated cell sorting (MACS) using the following Biolegend kits: cat. no. 480060 for monocytes, cat. no. 480054 for NK cells, cat. no. 480082 for B cells, cat. no. 480022 for T cells. Granulocytes (mostly neutrophils) are extracted from the bottom layer, whereby the erythrocytes are eliminated by water lysis for 30 s, followed by the addition of 10 vol% of 10x PBS to stop lysis. After cell isolation, monocytes, NK cells, B cells, and T cells are stored in R10 medium at 4 °C for 24 h, whereas neutrophils are used immediately. Purity of at least 85% for all isolated primary immune cell subsets (NK, T cells, B cells, monocytes, and neutrophils) are confirmed by flow cytometry (*SI Appendix, Methods*).

NK Cell IL-2 Activation. After 24 h storage at 4 °C, primary NK cells are incubated at 37 °C in R10 medium with or without 200 IU/mL human IL-2 cytokine for 1 h, 24 h, 48 h, or 72 h (Fig. 4 *E* and *F* and *SI Appendix*, Fig. S6) in a tissue-culture treated 24-well plate (Corning).

Ex Vivo Expansion of NK Cells. NK cells are ex-vivo expanded from PBMCs as previously described (24, 42, 43). PBMCs are isolated from healthy donors after oral and written informed consent (Department of Transfusion Medicine, University Hospital Erlangen, Germany; IRB approval number 147_13B and 22-314-Bp), In brief, PBMCs are cultured in the presence of irradiated K562-mbIL15-41BBL feeder cells (gift from Prof. D. Campana, Department of Pediatrics, University Hospital of Singapore) for 14 d in RPMI 1640 medium supplemented with 10% fetal bovine serum, 20 μg/mL gentamycin, 1% L-glutamine, and 200 IU/mL human IL-2 cytokine.

Collagen Gel Preparation. Immune cells are suspended in a collagen solution that is prepared at a temperature of 4 °C from a 2:1 mixture of rat tail collagen (Collagen R, 2 mg/mL, Matrix Bioscience) and bovine skin collagen (Collagen G, 4 mg/mL, Matrix Bioscience). We then add 10% (vol/vol) sodium bicarbonate (23 mg/mL) and 10% (vol/vol) 10× cRPMI (Gibco), and dilute the solution to a collagen concentration of 0.6 mg/mL, 1.2 mg/mL, or 2.4 mg/mL with a dilution medium containing 1 volume part $NaHCO_3$, 1 part 10 × cRPMI and 8 parts H_2O adjusted to pH 9 using NaOH. After polymerization at 37 °C, 5% CO_2, and 95% RH for 1 h, 1 to 3 mL cell culture medium or PBS is added (*SI Appendix, Methods*).

Manipulation of Cell–Matrix Adhesion. Cell adhesion on collagen fibers (Fig. 5 *A–D*) is prevented either by adding pluronic surfactant (1 vol% in PBS, Sigma-Aldrich, cat. no. 9003-11-6), or by calcium ion chelation with 5 mM ethylenediaminetetraacetic acid (EDTA, Roth, cat. no. 8040.3) in PBS. As a control, PBS is used.

Inhibition of Rho-kinase on NK92 cells (Fig. 3) is performed with Y-27632 Rock-inhibitor (Sigma-Aldrich, cat. no. 129830-38-2) dissolved in DMSO (Sigma-Aldrich, cat. no. 67-68-5) at a stock concentration of 1 mM. Y-27632 Rock-inhibitor is diluted in cell culture medium to a final concentration of 10 μM. Inhibition of myosin in NK92 cells (Fig. 3) is performed with blebbistatin (Sigma-Aldrich, cat. no. 856925-71-8) dissolved in DMSO at a stock concentration of 10 mM and mixed with cell culture medium to a final concentration of 3 μM. As control, DMSO is mixed in cell culture medium to a final concentration of 0.075 vol%.

Cells are mixed in collagen gel as described above. 2 mL of the PBS-drug solution (pluronic, EDTA, Y-27632, blebbistatin) or 2 mL of PBS with or without DMSO as control are added to the cell samples one hour after initiating collagen polymerization. Cells are incubated for 1 h before measurements.

For integrin blocking or integrin activation with antibodies (Fig. 5 *G* and *H* and *SI Appendix*, Fig. S9), we incubate 5-6*105 NK92 cells prior to mixing them into collagen for one hour in serum-free cell culture medium at 37 °C with or without the following antibodies: 10 μg/mL anti-integrin activating β1 (CD29) antibody (Biolegend, cat. no. 303002) and the corresponding IgG1 isotype (Biolegend, cat. no. 400101) as negative control; anti-integrin blocking β1 antibody (P5D2, Abcam, cat. no. ab24693) or anti-integrin blocking β2 (CD18) antibody (Merck, cat. no. CBL158), and the corresponding IgG1 isotype (rndsystems, cat. no. MAB002). After incubation with the antibodies, we mix the NK92 cells in collagen gel as described above.

Manipulation of Microtubules. Destabilization of microtubules in NK92 cells (Fig. 6) is performed with nocodazole (Biomol, Cay13857-10) dissolved in DMSO at a stock concentration of 10 mM. Serum-free cell culture medium is either mixed with nocodazole to a final concentration of 10 μM or mixed with DMSO to a final concentration of 0.1% (DMSO control). 300,000 NK92 cells are incubated for 10 min with serum-free cell culture medium with or without nocodazole. Subsequently, the cells are washed with serum-free cell culture medium and mixed in collagen gel as described above. After one hour of polymerization, 1 mL of the serum-free cell culture medium solution with or without nocodazole is added to the gel.

Carbomer Hydrogel Preparation. Carbomer hydrogel (Fig. 5 *A–D* and *SI Appendix*, Fig. S8) is prepared by mixing 9 mg carbomer powder (Ashland 980 carbomer, Covington) with 1 mL R10 medium. The pH is titrated to a value of 7.4 with 10 M NaOH. The carbomer solution is incubated at 37 °C and 5% CO_2 for at least one hour for equilibration. The migration assay is started directly after mixing 300,000 cells in 2 mL of 9 mg/mL carbomer in each well of a tissue-culture treated 6-well plate (Corning).

Brightfield Time-Lapse Imaging. For the high-throughput 3D migration assay, the well plate is transferred to a motorized microscope (Leica DMi6000B, equipped with a 10x 0.25 NA Leica objective and an Infinity III CCD camera, Lumenera) with a stage incubation chamber (Tokai HIT model: WSKMX) after gel preparation (*SI Appendix*, Table S1) and polymerization. We perform z-scans (10 μm apart) through the 1 mm thick gel every 15 s for a duration of 2.5 min for primary immune cells or for a duration of 5 min for ex-vivo expanded NK cells and NK92 cells. For each condition, we repeat this scanning procedure for 10 fields-of-view in sequence. For analysis, we detect individual cells using a convolutional neural network based on the U-Net architecture (44) (*SI Appendix, Methods*). For the high-resolution time-lapse images shown in Fig. 2 and Movies S6–S9 were recorded using a RAMM microscope system (Applied Scientific Instrumentation) equipped with a 60x 1.00 NA Olympus water-immersion objective (*SI Appendix, Methods*).

Single Cell 3-D Traction Force Microscopy. 3D traction force microscopy is performed as described in Refs. 14, 23. In brief, we pipette 3 mL collagen (0.6 to 2.4 mg/mL) solution with 200,000 cells into a cell culture-treated 35 mm Nunc Petri dish (ThermoFisher Scientific). After polymerization of the gel, 2 mL of cell culture medium are added. We image z-stacks around single cells with a cubic

volume of $(123\ \mu m)^3$ every 60 s using a confocal microscope (Leica DM 6000 CFS with HCX APO L 20x/1,00 W objective) equipped with a galvanometric stage and a resonance scanner (*SI Appendix, Methods*). We select elongated cells for traction force measurements specifically, as these are likely to be motile. From the recorded 3D reflection-channel image stacks, we reconstruct cell-induced traction forces using the SAENOPY Python software package (14) (*SI Appendix, Methods*). Data obtained in 3D traction force microscopy experiments shown in Fig. 3 *A* and *B* have previously been reported in the work by Böhringer et al. (14).

Bayesian Filtering of Cell Trajectories. Bayesian filtering of the individual NK cell trajectories is employed as described in Ref. 26, but adapted to the fast-moving immune cells. In particular, we use the probabilistic programming framework *bayesloop* to infer the temporal evolution of the filtered cell speed and the filtered directional persistence based on an autoregressive process of first order from a series of (x_t, y_t)-coordinates that are obtained from the TFM experiments (*SI Appendix, Methods*).

Data, Materials, and Software Availability. The 3D traction force microscopy method used in this work is implemented in the Python package *SAENOPY v0.7.4* (14). The Bayesian filtering of cell trajectories is implemented in the Python package *bayesloop* (26). The detection and tracking of immune cells in the high-throughput migration assays is implemented in custom Python scripts that are open source under the MIT License and are hosted on Github (45). The figures in this study have been created using the Python packages matplotlib (46) and Pylustrator (47). All study data are included in the article and/or supporting information.

ACKNOWLEDGMENTS. This work was supported by the NIH Grant HL120839. We acknowledge the support by the Deutsche Forschungsgemeinschaft (DFG, German Research Foundation) project number 540981488 and FA 336/20-1 to T.C. and B.F., and project number 460333672–CRC 1540 Exploring Brain Mechanics (subprojects A01, B01, and C05) to L.B., S.B. and B.F. We acknowledge the support by the DFG (FA 336-12/1, TRR-SFB 225) project 326998133 (subprojects A01, B09, and C02) to D.B., S.B. and B.F. and subproject C05 (TRR225) to R.S. We acknowledge the support by the IZKF junior project J108 to N.H. We thank Dario Campana, Andreas Baur, and Felix Rico for providing cell lines.

Author affiliations: [a]Department of Physics, Friedrich-Alexander University Erlangen-Nürnberg, Erlangen 91058, Germany; [b]Department of Genetics, Friedrich-Alexander University Erlangen-Nürnberg, Erlangen 91058, Germany; [c]Institute of Pathology, University Hospital Erlangen, Erlangen 91054, Germany; [d]Department of Gynecology and Obstetrics, University Hospital Erlangen, Erlangen 91054, Germany; [e]Department of Radiation Oncology, University of Maryland School of Medicine, Baltimore, MD 21201; [f]Comprehensive Cancer Center Erlangen-European Metropolitan Area of Nürnberg, University Hospital Erlangen, Erlangen 91054, Germany; [g]Department of Pediatrics and Adolescent Medicine, University Hospital Erlangen, Erlangen 91054, Germany; [h]Department of Dermatology, University Hospital Erlangen, Erlangen 91054, Germany; [i]Deutsches Zentrum Immuntherapie, Friedrich-Alexander University Erlangen-Nürnberg, Erlangen 91054, Germany; and [j]Department of Mechanical Engineering, Friedrich-Alexander University Erlangen-Nürnberg, Erlangen 91058, Germany

1. T. A. Springer, Traffic signals for lymphocyte recirculation and leukocyte emigration: The multistep paradigm. *Cell* **76**, 301–314 (1994).
2. T. Lämmermann *et al.*, Rapid leukocyte migration by integrin-independent flowing and squeezing. *Nature* **453**, 51–55 (2008).
3. P. Friedl, P. B. Noble, K. S. Zänker, T lymphocyte locomotion in a three-dimensional collagen matrix. Expression and function of cell adhesion molecules. *J. Immunol.* **154**, 4973–4985 (1995).
4. P. Friedl, F. Entschladen, C. Conrad, B. Niggemann, K. S. Zänker, CD4+ T lymphocytes migrating in three-dimensional collagen lattices lack focal adhesions and utilize β1 integrin-independent strategies for polarization, interaction with collagen fibers and locomotion. *Eur. J. Immunol.* **28**, 2331–2343 (1998).
5. K. Wolf, R. Müller, S. Borgmann, E.-B. Bröcker, P. Friedl, Amoeboid shape change and contact guidance: T-lymphocyte crawling through fibrillar collagen is independent of matrix remodeling by MMPs and other proteases. *Blood* **102**, 3262–3269 (2003).
6. P. Friedl, S. Borgmann, E.-B. Bröcker, Amoeboid leukocyte crawling through extracellular matrix: Lessons from the Dictyostelium paradigm of cell movement. *J. Leukoc. Biol.* **70**, 491–509 (2001).
7. C. T. Mierke, B. Frey, M. Fellner, M. Herrmann, B. Fabry, Integrin α5β1 facilitates cancer cell invasion through enhanced contractile forces. *J. Cell Sci.* **124**, 369–383 (2011).
8. J. Steinwachs *et al.*, Three-dimensional force microscopy of cells in biopolymer networks. *Nat. Methods* **13**, 171–176 (2016).
9. M. Cóndor *et al.*, Breast cancer cells adapt contractile forces to overcome steric hindrance. *Biophys. J.* **116**, 1305–1312 (2019).
10. J. Renkawitz *et al.*, Adaptive force transmission in amoeboid cell migration. *Nat. Cell Biol.* **11**, 1438–1443 (2009).
11. M. Hons *et al.*, Chemokines and integrins independently tune actin flow and substrate friction during intranodal migration of T cells. *Nat. Immunol.* **19**, 606–616 (2018).
12. K. M. Yamada, M. Sixt, Mechanisms of 3D cell migration. *Nat. Rev. Mol. Cell Biol.* **20**, 738–752 (2019).
13. D. J. Fowell, M. Kim, The spatio-temporal control of effector T cell migration. *Nat. Rev. Immunol.* **21**, 582–596 (2021).
14. D. Böhringer *et al.*, Dynamic traction force measurements of migrating immune cells in 3D biopolymer matrices. *Nat. Phys.* **20**,1823 (2024), 10.1038/s41567-024-02632-8.
15. M. Fénelon *et al.*, Applications of human amniotic membrane for tissue engineering. *Membranes* **11**, 387 (2021).
16. C. Touboul *et al.*, Mesenchymal stem cells enhance ovarian cancer cell infiltration through IL6 secretion in an amniochorionic membrane based 3D model. *J. Transl. Med.* **11**, 28 (2013).
17. B. Chen *et al.*, The mechanical properties of amniotic membrane influence its effect as a biomaterial for ocular surface repair. *Soft Matter* **8**, 8379–8387 (2012).
18. H. Niknejad, T. Deihim, M. Solati-Hashjin, H. Peirovi, The effects of preservation procedures on amniotic membrane's ability to serve as a substrate for cultivation of endothelial cells. *Cryobiology* **63**, 145–151 (2011).
19. J. Swift *et al.*, Nuclear lamin-A scales with tissue stiffness and enhances matrix-directed differentiation. *Science* **341**, 1240104 (2013).
20. N. R. Lang *et al.*, Estimating the 3D pore size distribution of biopolymer networks from directionally biased data. *Biophys. J.* **105**, 1967–1975 (2013).
21. L. Ruggeri *et al.*, Effectiveness of donor natural killer cell alloreactivity in mismatched hematopoietic transplants. *Science* **295**, 2097–2100 (2002).
22. T. J. Laskowski, A. Biederstädt, K. Rezvani, Natural killer cells in antitumour adoptive cell immunotherapy. *Nat. Rev. Cancer* **22**, 557–575 (2022).
23. M. Cóndor, J. Steinwachs, C. Mark, J. M. García-Aznar, B. Fabry, Traction force microscopy in 3-dimensional extracellular matrix networks. *Curr. Protoc. Cell Biol.* **75**, 10.22.1–10.22.20 (2017).
24. C. Mark *et al.*, Cryopreservation impairs 3-D migration and cytotoxicity of natural killer cells. *Nat. Commun.* **11**, 5224 (2020).
25. C. Metzner *et al.*, Superstatistical analysis and modelling of heterogeneous random walks. *Nat. Commun.* **6**, 7516 (2015).
26. C. Mark *et al.*, Bayesian model selection for complex dynamic systems. *Nat. Commun.* **9**, 1803 (2018).
27. P. E. Olofsson *et al.*, Distinct migration and contact dynamics of resting and IL-2–activated human natural killer cells. *Front. Immunol.* **5**, 80 (2014).
28. N. Q. Balaban *et al.*, Force and focal adhesion assembly: A close relationship studied using elastic micropatterned substrates. *Nat. Cell Biol.* **3**, 466–472 (2001).
29. D. Riveline *et al.*, Focal contacts as mechanosensors: externally applied local mechanical force induces growth of focal contacts by an mdia1-dependent and ROCK-independent mechanismâœ. *J. Cell Biol.* **153**, 1175–1186 (2001).
30. T. Tharmalingam, H. Ghebeh, T. Wuerz, M. Butler, Pluronic enhances the robustness and reduces the cell attachment of mammalian cells. *Mol. Biotechnol.* **39**, 167–177 (2008).
31. J.-Y. Kim, J.-Y. Song, E.-J. Lee, S.-K. Park, Rheological properties and microstructures of carbopol gel network system. *Colloid Polym. Sci.* **281**, 614–623 (2003).
32. T. Bhattacharjee, T. E. Angelini, 3D T cell motility in jammed microgels. *J. Phys. D. Appl. Phys.* **52**, 024006 (2019).
33. A. Reversat *et al.*, Cellular locomotion using environmental topography. *Nature* **582**, 582–585 (2020).
34. R. Garnotel *et al.*, Human blood monocytes interact with type I collagen through αxβ2 integrin (CD11c-CD18, gp150-95). *J. Immunol.* **164**, 5928–5934 (2000).
35. R. Zhao *et al.*, Targeting the microtubule-network rescues CTL killing efficiency in dense 3D matrices. *Front. Immunol.* **12**, 729820 (2021).
36. E. D. Tabdanov *et al.*, Engineering T cells to enhance 3D migration through structurally and mechanically complex tumor microenvironments. *Nat. Commun.* **12**, 2815 (2021).
37. A. Rape, W. Guo, Y. Wang, Microtubule depolymerization induces traction force increase through two distinct pathways. *J. Cell Sci.* **124**, 4233–4240 (2011).
38. J. Jacobelli, F. C. Bennett, P. Pandurangi, A. J. Tooley, M. F. Krummel, Myosin-IIA and ICAM-1 regulate the interchange between two distinct modes of T cell migration1. *J. Immunol.* **182**, 2041–2050 (2009).
39. R. A. Jannat, M. Dembo, D. A. Hammer, Traction forces of neutrophils migrating on compliant substrates. *Biophys. J.* **101**, 575–584 (2011).
40. A. Caillier, D. Oleksyn, D. J. Fowell, J. Miller, P. W. Oakes, T cells use focal adhesions to pull themselves through confined environments. *J. Cell Biol.* **223**, e202310067 (2024).
41. P. Reis-Rodrigues *et al.*, Global coordination of protrusive forces in migrating immune cells. bioXriv [Preprint] (2024), 10.1101/2024.07.26.605242.
42. C. Imai, S. Iwamoto, D. Campana, Genetic modification of primary natural killer cells overcomes inhibitory signals and induces specific killing of leukemic cells. *Blood* **106**, 376–383 (2005).
43. C. J. Voskens *et al.*, Ex-vivo expanded human NK cells express activating receptors that mediate cytotoxicity of allogeneic and autologous cancer cell lines by direct recognition and antibody directed cellular cytotoxicity. *J. Exp. Clin. Cancer Res.* **29**, 134 (2010).
44. O. Ronneberger, P. Fischer, T. Brox, U-Net: Convolutional networks for biomedical image segmentation (2015), http://arxiv.org/abs/1505.04597.
45. N. Huhn *et al.*, Immune cell migration analysis in python. GitHub. https://github.com/fabrylab/immune_cell_migration. Deposited 4 February 2026.
46. J. D. Hunter, Matplotlib: A 2D graphics environment. *Comput. Sci. Eng.* **9**, 90–95 (2007).
47. R. Gerum, Pylustrator: Code generation for reproducible figures for publication. *J. Open Source Softw.* **5**, 1989 (2020).